

Chapter 3

Simulation programs for the analysis of multilayer media

In this chapter, we present the software realized for the mathematical study and design of multilayers. Although different methods exist for the simulation of these structures, all the programs presented here are based on the transfer matrix method. Firstly, the transfer matrix method is explained in detail and its mathematical bases are presented. This method is compared with two other ones that can be also used for this purpose. After that, the realized simulation programs based on the transfer matrix method are explained in detail. Their selectable variables and the optical properties calculated with each one are presented. Finally, the performance of the programs is evaluated by comparing the simulated optical responses of widely reported multilayer structures (Distributed Bragg Reflectors and microcavities) with the ones obtained in the literature.

3.1. Mathematical methods for the analysis and simulation of multilayers

The development of methods for analyzing the multilayers is essential, if we want to understand their fundamental properties. Any experimental exploration of the multilayers must be accompanied by a quantitative theoretical analysis so that the most interesting cases can be identified, the experimental measurements interpreted, and stable designs for successfully operating devices be found. This section provides an outline of the most widely used numerical techniques that make it possible to determine the optical properties of multilayers. The first, the Transfer Matrix method is the method used for the analysis of the multilayers presented in this work, for this reason it is presented in detail whereas the rest of methods are briefly explained.

3.1.1. Transfer Matrix Method (TMM)

This is the most widely used method for the mathematical study of wave transmission in one-dimensional structures because it allows the calculation of band diagrams [149], reflectivity and transmission spectra [150], emission spectra [44], guided modes [126] and the modelization of porosity and thickness gradients [85].

To study the reflection and the transmission of electromagnetic radiation through a multilayer with the TMM method, we consider a one-dimensional structure consisting of alternating porous silicon layers of different refractive indices coupled to a homogeneous medium characterized by refractive index n_0 at the interface. Fig. 3.1 shows this structure, where n_1 and n_2 are the layers refractive index, h_1 and h_2 are the thicknesses of the respective layers and Λ is the period of the structure ($\Lambda = h_1 + h_2$).

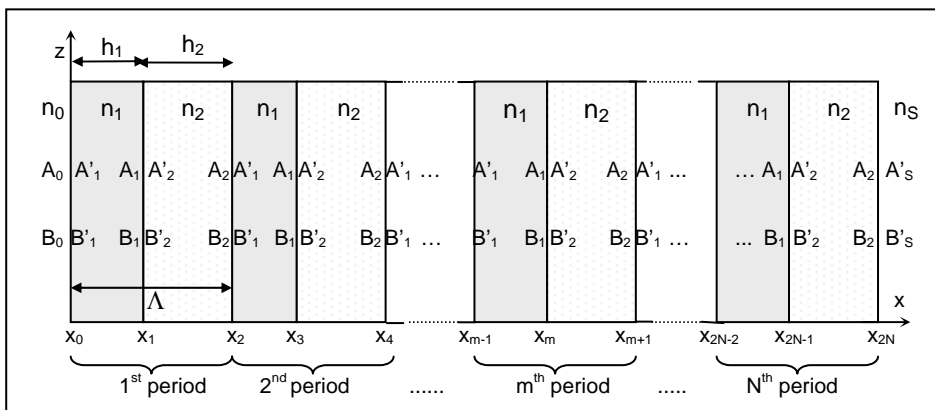


Fig. 3.1. Schematic of a multilayer system. $A(x)$ represent the amplitude of the right-traveling-wave and $B(x)$ that of the left-traveling one. Note that $A(x)$ and $B(x)$ are not continuous at the interfaces. It is a periodic structure made of two layers, 1 and 2. The thickness of each layer is h_m , n_m is the refractive index and Λ is the period. The structure is coupled to a homogeneous medium characterized by n_0 (initial medium) and n_s (final medium).

The dielectric structure is defined by

$$n(x) = \begin{cases} n_0, & x < x_0 \\ n_1, & x_0 < x < x_1 \quad \text{with } x_1 = x_0 + h_1 \\ n_2, & x_1 < x < x_2 \quad \text{with } x_2 = x_0 + \Lambda = x_1 + h_2 \\ \vdots & \\ n_s, & x_{2N} < x \quad \text{with } x_{2N} = x_0 + N\Lambda = x_{2N-1} + h_2 \end{cases} \quad (3.1)$$

with $n(x) = n(x + \Lambda)$. n_s is the substrate refractive index, n_0 is that of the incident medium and n_m is the refractive index of the m layer. Layer thicknesses are related to x_m by $h_m = x_m - x_{m-1}$ ($m = 1..2N$).

The electric field of a general plane-wave solution can be written as $E = E(x)e^{i(\omega t - \beta z)}$, where the electric field distribution $E(x)$ can be written as

$$E(x) = \begin{cases} A_0 e^{-ik_{0x}(x-x_0)} + B_0 e^{ik_{0x}(x-x_0)}, & x < x_0 \\ A_m e^{-ik_{mx}(x-x_m)} + B_m e^{ik_{mx}(x-x_m)}, & x_{m-1} < x < x_m, \\ A'_s e^{-ik_{sx}(x-x_{2N})} + B'_s e^{ik_{sx}(x-x_{2N})}, & x_{2N} < x \end{cases} \quad (3.2)$$

where k_{mx} is the x component of the wave vectors $k_{mx} = \omega n_m \cos \theta_m / c$ and θ_m is the ray angle in each layer. A_m and B_m represent the amplitude of the plane waves at interface $x=x_m$ (see Fig. 3.1).

If the two general amplitudes of $E(x)$ are represented as column vectors, the plane waves at different layers can be related by

$$\begin{pmatrix} A_{m-1} \\ B_{m-1} \end{pmatrix} = D_{m-1}^{-1} D_m \begin{pmatrix} A'_m \\ B'_m \end{pmatrix} = D_{m-1}^{-1} D_m P_m \begin{pmatrix} A_m \\ B_m \end{pmatrix} \quad m=1,2,\dots,2N+1 \quad (3.3)$$

where matrices D_m are the dynamical matrices given by

$$D_m = \begin{cases} \begin{pmatrix} 1 & 1 \\ n_m \cos \theta_m & -n_m \cos \theta_m \end{pmatrix} & \text{for TE wave} \\ \begin{pmatrix} \cos \theta_m & \cos \theta_m \\ n_m & -n_m \end{pmatrix} & \text{for TM wave} \end{cases} \quad (3.4)$$

and P_m is the propagation matrix, that can be written as

$$P_m = \begin{pmatrix} e^{ik_{mx}h_m} & 0 \\ 0 & e^{-ik_{mx}h_m} \end{pmatrix} \quad (3.5)$$

The relation between A_0, B_0 and A'_s, B'_s can thus be written as

$$\begin{pmatrix} A_0 \\ B_0 \end{pmatrix} = D_0^{-1} [D_1 P_1 D_1^{-1} D_2 P_2 D_2^{-1}]^N D_s = \begin{pmatrix} M_{11} & M_{12} \\ M_{21} & M_{22} \end{pmatrix} \begin{pmatrix} A'_s \\ B'_s \end{pmatrix} \quad (3.6)$$

where N is the number of periods in the structure.

3.1.1.1. Reflectance and transmittance of the multilayer

The reflectance and transmittance of monochromatic plane waves through the multilayer structure are calculated from the matrix elements.

If the light is incident from medium 0, the reflection and transmission coefficients are defined as

$$r = \left(\frac{B_0}{A_0} \right)_{B_s=0} \quad (3.7)$$

$$t = \left(\frac{A_s}{A_0} \right)_{B_s=0}$$

Using the matrix equation (3.6) and following the definitions in Eq. (3.7), we obtain

$$r = \frac{M_{21}}{M_{11}} \quad (3.8)$$

$$t = \frac{1}{M_{11}}$$

Reflectance is given by

$$R = |r|^2 = \left| \frac{M_{21}}{M_{11}} \right|^2 \quad (3.9)$$

provided medium 0 is lossless.

If the bounding media (0,s) are both pure dielectric with real n_s and n_0 , transmittance T is given by

$$T = \frac{n_s \cos \theta_s}{n_0 \cos \theta_0} |t|^2 = \frac{n_s \cos \theta_s}{n_0 \cos \theta_0} \left| \frac{1}{M_{11}} \right|^2 \quad (3.10)$$

3.1.1.2. Bloch waves and band structures

Wave propagation in periodic media is very similar to the motion of electrons in crystalline solid. In fact, formulation of the Kroning Penny model used in elementary band theory of solids is mathematically identical to that of the electromagnetic radiation in periodic layered media. Thus, some of the physical concepts used in solid-state physics such as Bloch waves, Brillouin zones and forbidden bands can also be used here. A periodic layered medium is equivalent to a one-dimensional lattice that is invariant under lattice translation. In other words $n^2(x+\Lambda)=n^2(x)$, where Λ is the period

According to the Floquet theorem, solutions of wave equations for a periodic medium are of the form [151] $E_K(x,z)=E_K(x)e^{-i\beta z}e^{-iKx}$, where $E_K(x+\Lambda)=E_K(x)$. The subscript K indicates that the function $E_K(x)$ depends on K . The constant K is known as the Bloch wave number. The problem is thus that of determining K and $E_K(x)$.

In term of our column vector representation and from Eq. (3.2), the periodic condition $E_K(x+\Lambda)=E_K(x)$ for the Bloch wave is simply

$$\begin{pmatrix} A_1 \\ B_1 \end{pmatrix}_{n \text{ period}} = e^{-iK\Lambda} \begin{pmatrix} A_1 \\ B_1 \end{pmatrix}_{n-1 \text{ period}} \quad (3.11)$$

From the matrix expression (3.3), the unit cell of the periodic multilayer can be defined as

$$\begin{pmatrix} A_1 \\ B_1 \end{pmatrix}_{n-1 \text{ period}} = D_1^{-1}D_2P_2D_2^{-1}D_1P_1 \begin{pmatrix} A_1 \\ B_1 \end{pmatrix}_{n \text{ period}} = \begin{pmatrix} S & T \\ U & V \end{pmatrix} \begin{pmatrix} A_1 \\ B_1 \end{pmatrix}_{n \text{ period}} \quad (3.12)$$

It follows from this equation and Eq. (3.11) that the column vector of the Bloch wave satisfies the following eigenvalue problem:

$$\begin{pmatrix} S & T \\ U & V \end{pmatrix} \begin{pmatrix} A_1 \\ B_1 \end{pmatrix} = e^{iK\Lambda} \begin{pmatrix} A_1 \\ B_1 \end{pmatrix} \quad (3.13)$$

The phase vector $e^{iK\Lambda}$ is thus the eigenvalue of the translation matrix (S,T,U,V) and is given by

$$e^{iK\Lambda} = (1/2)(S+V) \pm \{[(1/2)(S+V)]^2 - 1\}^{1/2} \quad (3.14)$$

The eigenvectors corresponding to this eigenvalues are obtained from Eq. (3.13) and are

$$\begin{pmatrix} A_0 \\ B_0 \end{pmatrix} = \begin{pmatrix} T \\ e^{jK\Lambda} - S \end{pmatrix} \quad (3.15)$$

times the arbitrary constant. The Bloch waves that result from Eq. (3.15) can be considered as the eigenvectors of the translation matrix with eigenvalues $e^{\pm iK\Lambda}$ given by Eq. (3.14). The two eigenvalues in Eq. (3.14) are the inverse of each other since the translation matrix is unimodular. Eq. (3.14) gives the dispersion relation between ω , β and K for the Bloch function,

$$K(\beta, \omega) = (1/\Lambda) \cos^{-1}[(1/2)(S+V)] \quad (16)$$

Regimes where $|(1/2)(S+V)| < 1$ correspond to real K and thus to propagation Bloch waves; when $|(1/2)(S+V)| > 1$, however, $K = m\pi/\Lambda + iK_i$ which has an imaginary part K_i so that the Bloch wave is evanescent. These are the so-called forbidden bands of the periodic medium. The band edges are the regimes where $|(1/2)(S+V)| = 1$.

The dispersion relation can be also written as

$$\cos K\Lambda = \frac{1}{2}(S + V) = \cos k_1 d_1 \cos k_2 d_2 - \frac{1}{2}\varphi \sin k_1 d_1 \sin k_2 d_2 \quad (3.17)$$

where $\varphi = \frac{k_{2x}}{k_{1x}} + \frac{k_{1x}}{k_{2x}}$ for TE waves and $\varphi = \frac{n_2^2 k_{1x}}{n_1^2 k_{2x}} + \frac{n_1^2 k_{2x}}{n_2^2 k_{1x}}$ for TM waves, and

$$\beta = \omega n_m \sin\theta/c.$$

In order to study the omnidirectional band gap of a multilayer, the dispersion relation is calculated for all incidence angles, obtaining the projected band structure (PBS).

3.1.1.3. Advantages and drawbacks of the TMM

The TMM has many advantages. It is a very useful algorithm, very appropriate for reflectivity and transmission calculations of multilayer structures. It can take in values for the refractive index that are either real or complex. A real refractive index represents a lossless material whereas a complex refractive index can represent either one of two types of materials. If the imaginary part of the complex refractive index is negative then the material is absorptive. If it is positive then this is an indication of having a gain medium.

The TMM can also handle any number of layers in a multilayer structure. In addition, these layers can be ordered in any manner and there is no requirement that they should be periodic. Even if they are periodic, the unit cell that is repeated does not have to be composed of two layers only, but any number of layers. There is also no restriction on the thickness of any layer. The thickness and the refractive index of each layer can be defined independently. This makes the TMM most suitable for modelling structures formed by different periodic multilayers stacked together, since they are not fully periodic.

The TMM can handle structures having a high index contrast between their two composite materials contrast material systems. This makes the TMM suitable for modelling multilayer structures, which usually have a high index contrast between their composite materials.

The TMM has also some drawbacks. For example, it assumes that the plane perpendicular to the direction of propagation is infinite, meaning that each layer in a multilayer structure extends infinitely in both of its dimensions. Of course, this is unrealistic, so the layers that are modelled have to be wide enough to avoid errors from this assumption. The TMM calculates the field throughout the structure by propagating it from one layer to the other by matrix relations. As such, it depends greatly on the computational speed and is therefore limited by it. It lacks a mathematical expression that can relate the field between multiple layers, which would reduce the mathematical calculations required and consequently the computational time.

Another drawback of the TMM is that it is limited to continuous wave propagation and cannot handle pulse propagation. To model pulses, the TMM

must be combined with the Fourier Transform. Pulses are better modelled with other techniques such as the Finite Difference Time Domain method.

3.1.2. Plane Wave Method

Another way to calculate photonic band structures is to adapt the methods of electronic band structure calculations to the case of photonic crystals. The plane wave expansion method can be classified as one of the numerical techniques borrowed from solid state physics. However, it had to undergo various adjustments before it could be carried over to the photonic case. These adjustments reflect the differences between photonic and conventional crystals, such as the fact that the electromagnetic field is inherently vectorial by nature or that the “scattering potentials” of photonic atoms are known beforehand and do not have to be determined self-consistently.

The plane wave method is used to solve periodic electromagnetic problems, among them the modelization of periodic structures, because accurate and reliable results are obtained [152]. It is widely used to find the Bloch frequencies of infinite periodic structures [125,153,154].

This method uses the Fourier expansion in terms of harmonic functions (modes), defined by the reciprocal space vectors. By applying the Fourier expansion in terms of Bloch waves $H_k(r) = u_k(r)e^{ikr}$, the Maxwell’s equations are converted to an eigenvalue and eigenvector problem:

$$\Theta H(r) = \left(\frac{\omega}{c}\right)^2 H(r) \quad (3.18)$$

where $\Theta = \nabla \times \left(\frac{1}{\varepsilon(r)}\right) \nabla \times$ is the Maxwell’s operator. The $u_k(k)$ function is a periodic function that follows the structure periodicity.

The plane wave method is one of the first methods used, because it is easy to understand and computationally very straightforward to implement. It can be used to solve periodic problems in one, two and three dimensions. However, it has some serious limitations which restrict its usefulness. First, the

method fixes the wave vector \vec{k} and then determines the eigenfrequencies for this \vec{k} , so the method runs into difficulties if the dielectric constant is itself a function of frequency. Hence, structures that include metallic or other dispersive materials are beyond the scope of the plane wave method. Second, the key step in the method is the matrix diagonalization, so the computer time required scales like N^3 , where N is the number of plane waves used in the expansion. This scaling law is inefficient and renders the calculations impossibly time consuming when a large number of plane waves is required for more complex structures [155].

3.1.3. Finite Difference Time Domain

The finite difference time domain (FDTD) approach overcomes all the drawbacks of the plane wave method. It was first described by Yee in 1966 [156] and so has been known to the electrical engineering community for 40 years. The methodology and computational schemes for a variety of photonic problems can be found in the excellent book by Taflove [157].

The FDTD method is a general method for numerically solving the time-dependent Maxwell's equations in real space, approximating the space and time derivatives with finite differences. With the appropriate choice of the points at which the various field components are to be evaluated, the set of finite difference equations can be solved and the solution will satisfy the boundary [156].

It is a widely used technique for solving electromagnetic problems and has many advantages: the method is a direct solution of Maxwell's time-domain equations, consequently, it is a complete full-wave solution that contains no approximations; it is extremely general in the materials and geometries that it can analyze; and, finally, the memory requirements of FDTD are significantly less than other methods, like PWM [158].

The principal disadvantage of the classical implementation of FDTD is that all structures must conform to a Cartesian grid; consequently, all curved

surfaces must be modeled by a "stairstep" approximation, which can introduce errors in the results.

3.2. Development of the simulation programs

The simulation and study of the optical behavior of multilayer structures has been carried out with two programs especially developed. The optical behavior of multilayers is characterized by the reflectivity, transmission and absorption spectra, as well as by the band diagram. Omnidirectional mirrors are also characterized by the projected band structure (PBS), which determines the band diagram for all incident angles and for both polarizations.

The realized programs calculate all these characteristics using the transfer matrix method [151]. All the graphs that are presented in the next sections have been calculated using these simulation programs.

3.2.1. Program for the calculation of reflectivity, transmission, and absorption spectra.

The main objective of this program is to study the optical response of a multilayer before its fabrication. The simulated structures can be either all-dielectric or metallo-dielectric multilayers. The program is based on the transfer matrix method. In Fig. 3.2 we can observe the main program window, where the user can define all the parameters required for the simulation. These parameters are:

- **Incidence angle:** Angle between the propagation direction of the incident wave and the normal to the surface of the layers. This angle (θ) can go from 0 to 90 degrees.
- **Refractive index of the ambient medium:** the ambient medium is the medium from which the incident wave arrives to the surface of the multilayer.

- **Refractive index of the substrate:** the substrate can be either a material in case that the multilayer is stacked to the wafer or a medium if the multilayer is a membrane detached from the substrate.
- **Data plotted:** reflectivity, transmission, absorption or any combination of them.
- **Wavelength range:** the initial and the final values of the wavelength range to be studied and the step, all of them in nanometers.
- **Graphs:** the data calculated is plotted in two different graphs, one for TE polarization and the other for TM polarization. Each graph or both can be also plotted in a separate window selecting the check box “Plot in a separate window”, where the user can change the properties of the plot in the same way that any Matlab plot.

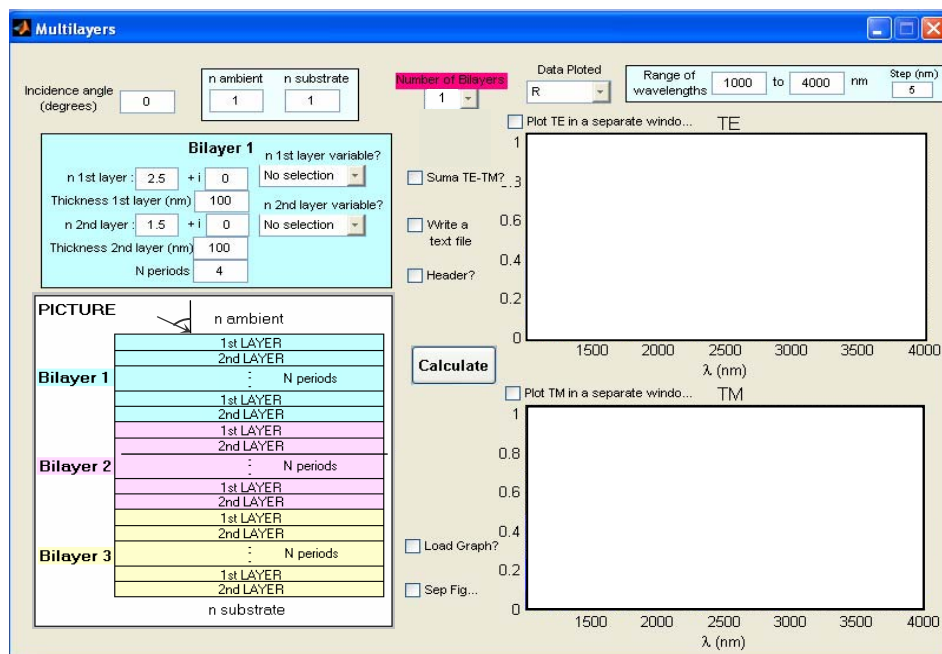


Fig. 3.2. Main program window. The schematic of a multilayer is presented to visually indicate the user the parameters that can be adjusted. The default values of the parameters can be observed.

- **Number of bilayers:** number of periodic multilayers stacked together that form the multilayer structure. This number can range from 1 to 6 bilayers. When the user chooses the number of bilayers of the structure, one frame for each bilayer appears in the program window with the parameters to be adjusted: refractive indices and thicknesses of the two layers and number of periods. An example with three bilayers is shown in Fig. 3.3.
- **Bilayer frame:** The parameters of each periodic bilayer are determined in this frame. These parameters are the **thicknesses** and **refractive indices** of the two materials that form the bilayer and the **number of periods**. The refractive index can be either constant (real or complex) or variable with the wavelength, in which case different materials can be selected from the popup menu **n layer variable?**: silver (Ag), aluminium (Al), gold (Au), copper (Cu), water (H₂O), magnesium fluoride (MgF₂), nickel (Ni), silicon nitride (Si₃N₄), and silicon dioxide (SiO₂). The variable refractive indices used for these materials have been obtained from [159]. The possibility to determine up to six different periodic bilayers stacked together makes it possible to simulate different multilayers.
- **Sum TE-TM:** The spectrum of a wave containing both polarizations is plotted in a separate graph when this check box is selected.
- **Write a text file:** Enables the possibility to save the data plotted in one or both graphs to a text file.
- **Header:** The text file with the results of the simulation can be written with or without a header. Selecting this check box, the text file is written with a header.
- **Load Graph:** Selecting this checkbox, the data from a text file can be also plotted with the simulated results. With this option, it is possible to compare simulations with measurements and different plots in an easy way.
- **Calculate:** Once all the parameters for the simulation have been selected, the program is executed pushing this button.

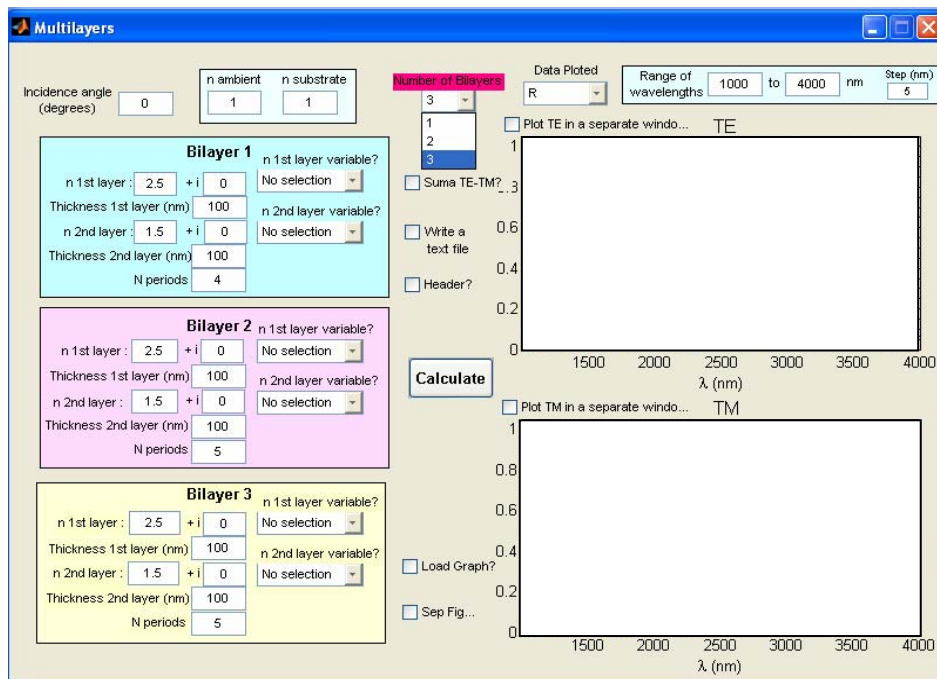


Fig. 3.3. Main program window. In this case the user has selected to simulate a structure formed by three bilayers.

Fig. 3.4 shows the simulation of a multilayer with two bilayers. The first bilayer consists of the repetition of two dielectric materials with constant refractive indices whereas the second bilayer is formed by a dielectric layer with constant refractive index and a silver layer. The refractive index of the silver layer is variable with the wavelength and the best way to simulate this material is to select its refractive index in the popup menu. The reflectivity spectrum of the multilayer is plotted in the graphs. We can also observe the difference between the TE and TM polarizations when the incidence angle is 50 degrees.

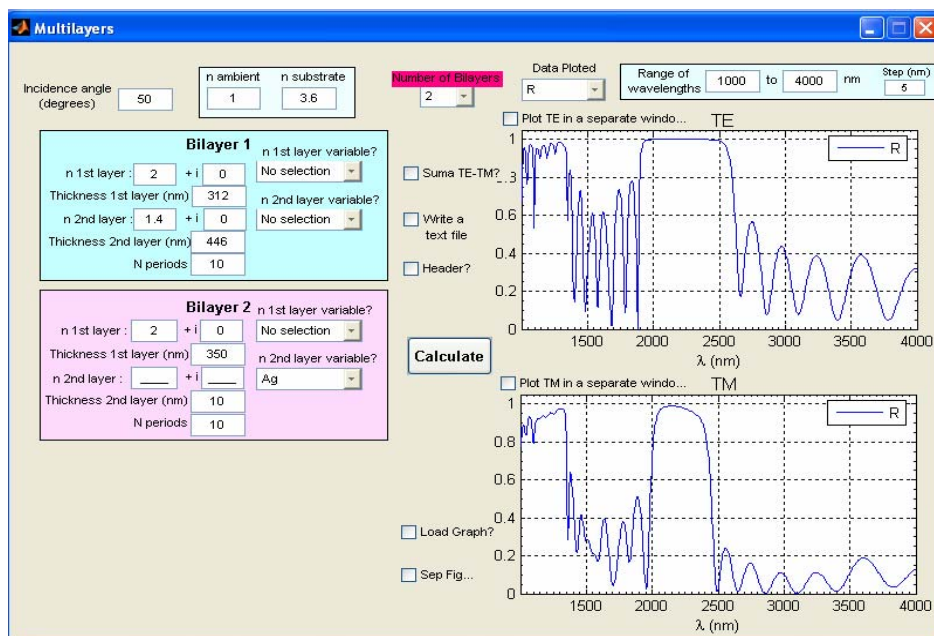


Fig. 3.4. Example of the simulation of a multilayer consisting of two periodic bilayers stacked together. In Bilayer 2 the second layer is silver, for this reason the corresponding refractive index variable with wavelength has been selected.

3.2.2. Program for the calculation of photonic band diagrams

The main objective of this program is to study the band diagram of a multilayer before its fabrication. It also compares the band diagram with the reflectivity or transmission spectra of the multilayer to confirm that there is an agreement between the calculated band diagram and the spectrum of the multilayer and to observe the influence of the finite number of periods on the bandgap edges. The program can also calculate the projected band structure (PBS) of the studied multilayer, which represents the band diagrams for all incidence angles from 0 to 90 degrees. This program is also based on the transfer matrix method.

In Fig. 3.5 we can observe the main window of this simulation program, where the user can define all the parameters for the simulation. The band diagram is a characteristic of infinite periodic multilayers therefore for the calculation of the band diagram and the PBS, the only required parameters are the ones presented in the frames named “Infinite periodic structure” and “Band diagram”:

- **Refractive index of the layers:** denoted by n 1st layer and n 2nd layer.
- **h_1 /period:** Thickness of the first layer normalized to the period thickness. Thus, h_1 /period can range from 0 to 1. The thickness of layer 2 is calculated from h_1 using: $h_2 = \text{period} - h_1$.
- **Maximum value of the normalized frequency:** maximum value of $(\omega\Lambda/2\pi c)$ for the calculation of the band diagram.
- **Plot PBS:** The projected band structure (PBS) of the multilayer is also plotted in a separated window when this check box is marked. In Fig. 3.6 the PBS calculated by the program is shown.

The band diagram calculated for this multilayer is plotted in the left side graph. This band diagram belongs to an infinite multilayer but the fabricated multilayers are finite, consequently it would be interesting to compare the high reflectivity (or low transmission) bands of the finite multilayer with the band diagram. For this reason, the right-side graphs show the reflection/transmission spectrum of the finite multilayer (upper graph) and the band diagram of the infinite multilayer (lower graph) for an easy comparison. For the calculation of the spectrum the next parameters are required:

- **Refractive index of the ambient medium:** the ambient medium is the medium from which the incident wave arrives to the surface of the multilayer.
- **Refractive index of the substrate:** the substrate can be either a material in case that the multilayer is stacked to the wafer or a medium if the multilayer is a membrane detached form the substrate.

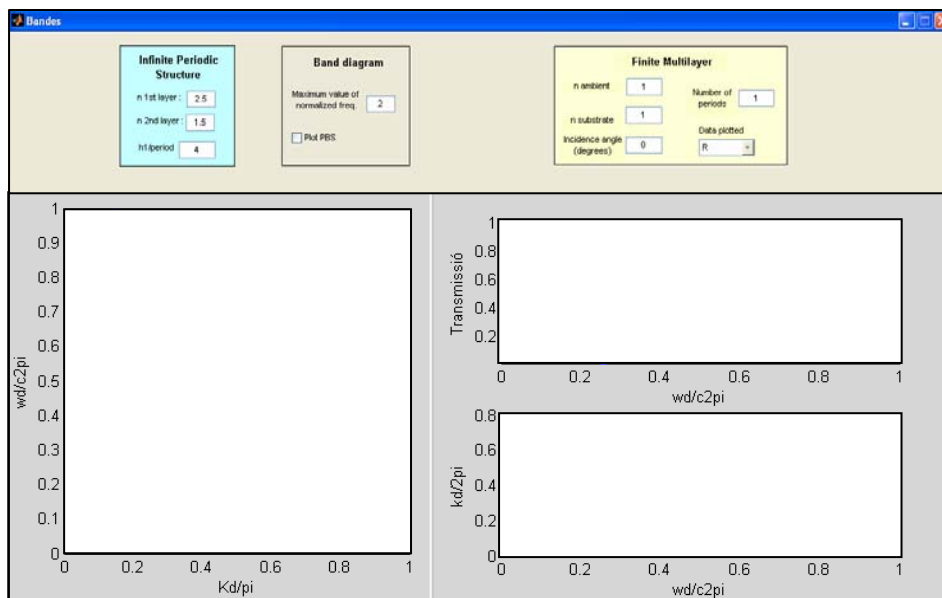


Fig. 3.5. Program for the calculations of the band diagram and projected band structure of a periodic multilayer. The reflectivity spectrum is also presented.

- **Incidence angle:** Angle between the propagation direction of the incident wave and the normal to the surface of the layers. From 0 to 90 degrees.
- **Number of periods** of the multilayer.
- **Data plotted:** reflectivity or transmission spectrum.

Fig. 3.6 shows the main program window with the results of the simulation for an example multilayer. The design parameters of the multilayer can be read in the window program. The comparison between the band diagram and the transmission spectrum indicates that, for this number of periods, the edges of the bandgaps are not sharp. For this reason, the ranges of frequencies with transmission zero are slightly narrower than the bandgaps of the infinite multilayer. In the next sections the relation between the sharpness of the band edges and the number of periods of the periodic multilayer is studied. The PBS

of the multilayer is plotted in a separate window and can be observed at the bottom of Fig. 3.6. The omnidirectional bandgap (black region) is also plotted.

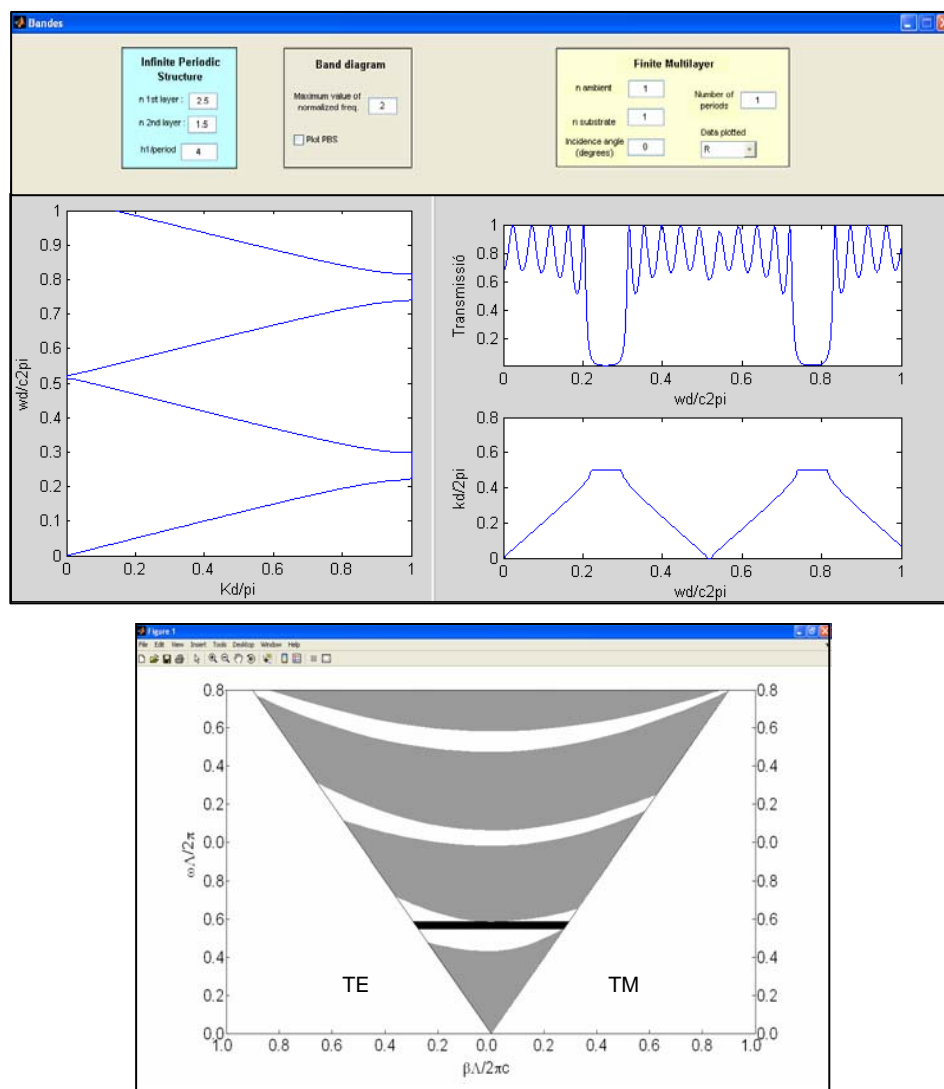


Fig. 3.6. Top: Example of the simulation of a multilayer using the explained program. Bottom: Window with the PBS of the infinite multilayer simulated.

All the different optical devices studied in this work have been analyzed using these two simulation programs.

3.3. Performance of the developed programs for the study of optical devices

In order to evaluate the performance of the developed programs explained in the previous section, different optical devices based on multilayers and widely reported in the literature have been simulated. The obtained spectra have been compared with the ones reported. These optical devices are Distributed Bragg Reflectors and microcavities. Besides, the developed programs have been used to study the influence of the different parameters of these devices on their optical behavior.

3.3.1. Distributed Bragg Reflectors (DBR)

These filters, as is explained in chapter 2, are characterized by a spectral region with a very high reflectivity, the so-called forbidden band or bandgap, centered at wavelength λ . This high reflectivity is due to the fact that all the beams that are reflected at the multiple interfaces of the multilayer have the same phase when they arrive to the top interface, interfering constructively. For wavelengths different to λ , the interference is not constructive and for this reason the reflectivity decreases.

3.3.1.1. Performance of the developed programs for the simulation of DBRs

The developed programs have been realized to theoretically study multilayers consisting of dielectric and/or metallic layers. To evaluate the performance of the programs, the spectra of two DBRs made of different materials have simulated. Firstly, a dielectric DBR, in concrete one of the porous silicon DBRs presented by Pavesi in [78], is simulated with the same

parameters used by the author. The reported DBR consists of two layers with $n_H=1.86$ and $n_L=1.27$ repeated 20 times. It is a $\lambda/4$ -DBR, so the optical thickness of the layers are $\lambda/4= n_H d_H=n_L d_L$ with $\lambda =600$ nm. For the simulations, the author considered no absorption, $n_{air}=1$ and refractive index of the substrate $n_{Subs}=4.1$. This structure has been simulated with our program and the reflectivity spectrum obtained is shown in Fig. 3.7 together with the spectrum reported in the literature. It can be observed that our simulated spectrum completely agrees with the spectrum reported in [78].

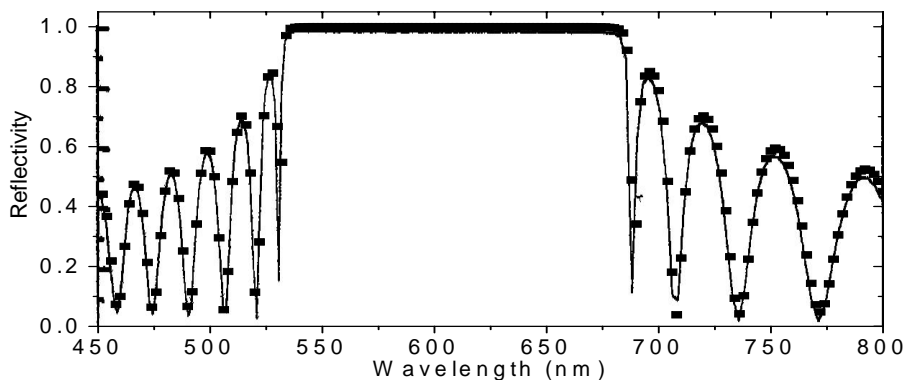


Fig. 3.7. Reflectivity spectrum of the porous silicon DBR simulated by Pavesi (After [78]) (solid line). It is compared with the simulated reflectivity spectrum obtained with our program for the same multilayer structure (symbols).

The developed programs can also simulate metallo-dielectric multilayers as the one presented by Scalora *et. al.* in [160]. In that work, the transmission spectrum of a multilayer consisting of a layer of silver and another of magnesium fluoride (MgF_2) repeated 4 times is studied. The thickness of the silver layer is 10 nm and the one of the MgF_2 layer is 110 nm. Fig. 3.8 shows the comparison between the transmission spectrum reported in the literature and

the one simulated with our program. It can be observed that the two spectra agree.

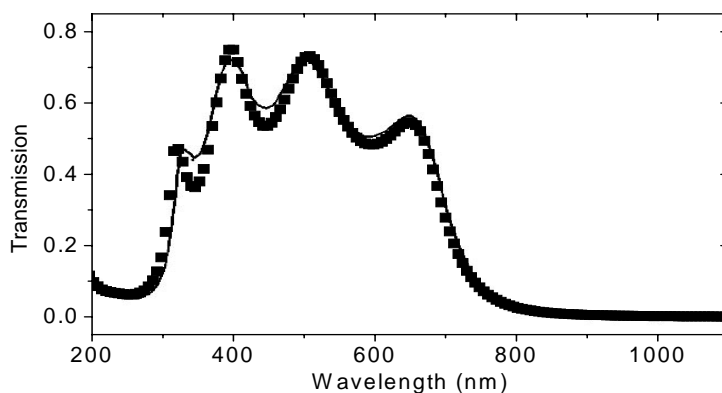


Fig. 3.8. Transmission spectrum of the metallo-dielectric multilayer simulated by Scalora (After [160]) (solid line). It can be compared with the transmission spectra simulated with our programs (symbols).

The agreement between the simulated spectra and the spectra reported in the literature confirms the properly performance of the developed programs and their suitability for the simulation of dielectric and metallo-dielectric multilayers.

3.3.1.2. Study of the DBR parameters

The simulation is a very helpful tool to study the influence of the different parameters of DBR on the reflectivity spectrum. These parameters are:

a) *Refractive index ratio n_H/n_L*

This ratio influences on the width and the sharpness of the DBR bandgap. The increase of the ratio n_H/n_L leads to the widening of the bandgap. This effect can be observed in Fig. 3.9, where the reflectivity spectra of three $\lambda/4$ -DBRs with different n_H/n_L ratio show a bandgap with different width. We can also observe that the band edges become sharper when the ratio increases.

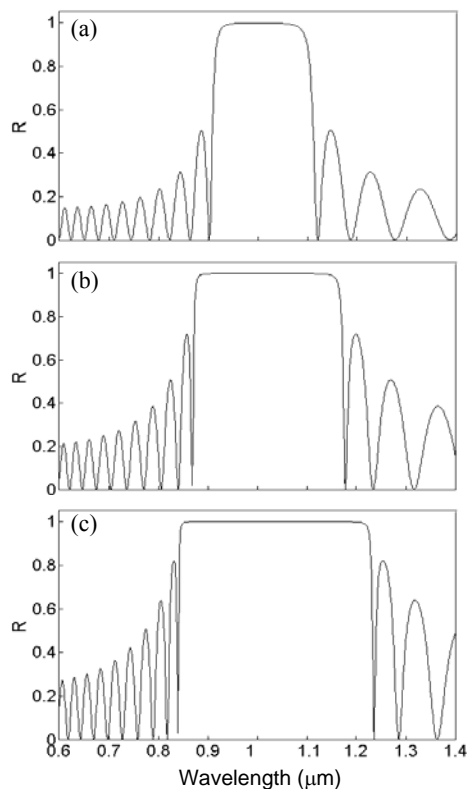


Fig. 3.9. Reflectivity spectrum for normal incidence of three different $\lambda/4$ -DBR with 15 periods. The thickness of the layers have been calculated to obtain a bandgap centered at $\lambda=1 \mu\text{m}$. The n_H/n_L ratio is a) 1.7/1.3, b) 2/1.3, c) 2.3/1.3.

The bandgap of these spectra are not symmetric around the central wavelength, in this case $1 \mu\text{m}$, because the symmetry can be observed when the magnitude of the x-axis is wavenumber instead of wavelength. To verify this symmetry, the three spectra of Fig. 3.9 are plotted in Fig. 3.10 using wavenumber for the x-axis.

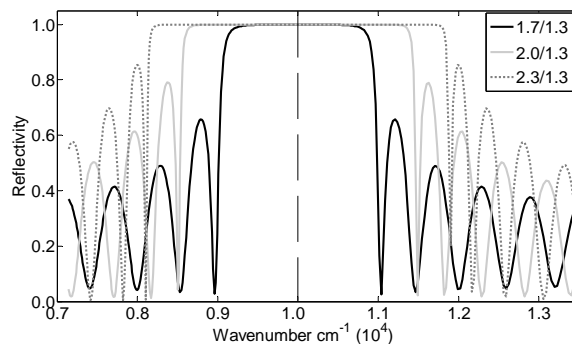


Fig. 3.10. Reflectivity spectrum for normal incidence of three different multilayers already presented in Fig. 3.9. In this case, the wavenumber is used for the x-axis. The symmetry of the bandgaps, centered at 1 cm^{-1} can be observed.

b) Number of periods of the multilayer

The number of periods (N) influences on different characteristics of the bandgap. The increase in the number of periods N leads to an increase of the reflectivity within the bandgap, and enlarges its width. The band edges also become sharper. Fig. 3.11 shows four $\lambda/4$ -DBR with $n_H=2.1$, $n_L=1.5$ and different number of periods N . We can observe that when N increases, the band edges of the filter are sharper and the reflectivity tends to the unity exponentially with N [161].

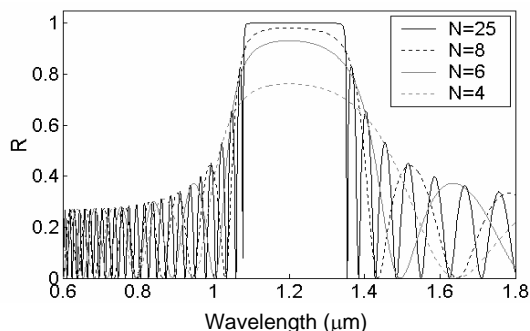


Fig. 3.11. Reflectivity spectrum of a $\lambda/4$ -DBR with $n_H=2.1$, $n_L=1.5$ and number of periods 4, 6, 8 and 25.

3.3.1.3. Design of a porous silicon DBR for 1.55 μm applications

The use of porous silicon for the study and design of DBR does not imply more difficulties than any other dielectric material. The main consequence of the use of porous silicon is that the range of refractive indices that can be obtained is limited due to the characteristics of the material. For this reason, the bandgap width of porous silicon DBR is limited because of the n_H/n_L ratio limitation. In order to obtain a DBR with a wide bandgap, two typical values, one of the highest and one of the lowest values of this refractive index range, have been chosen [19]: $n_H=2.5$ and $n_L=1.55$. The number of periods is high enough to obtain reflectivity near 1 within almost all the bandgap ($N=25$).

This DBR is designed to work for 1.55 μm applications, like all the porous silicon optical devices studied in this work. This wavelength is usually used for telecommunications applications. Since the bandgap of the $\lambda/4$ -DBR must be centered at 1.55 μm , the optical thickness of the layers must be $1.55 \mu\text{m}/4 = n_H h_H = n_L h_L$. According to this, the layer thicknesses are $h_H=155 \text{ nm}$ and $h_L=258.3 \text{ nm}$. The reflectivity spectrum of this DBR can be observed in Fig. 3.12. The bandgap width is around 500 nm for reflectivity higher than 99.9%. This would be one of the widest bandgaps obtainable with periodic porous silicon DBR centered at this wavelength.

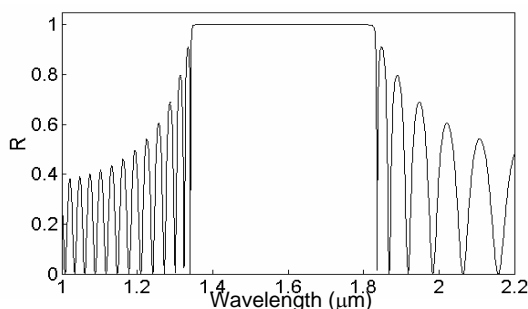


Fig. 3.12. Reflectivity spectrum of a porous silicon $\lambda/4$ -DBR for 1.55 μm applications. It has 25 periods, $n_H=2.5$, $n_L=1.55$, $h_H=155 \text{ nm}$ and $h_L=258.3 \text{ nm}$.

3.3.1.4. Reflectivity spectrum of stacked filters

Usually, the applications of DBR require wide bandgaps. As has been demonstrated in the previous section, the widening of the bandgap is obtained with the increase in the n_H/n_L ratio. Due to the limits of the n_H/n_L ratio for porous silicon, an easy way for obtaining enlarged bandgap reflectors is to stack together two or more reflectors. The reflectors used for the stack must have their bandgaps centered at different wavelengths but close enough to intersect one with the other.

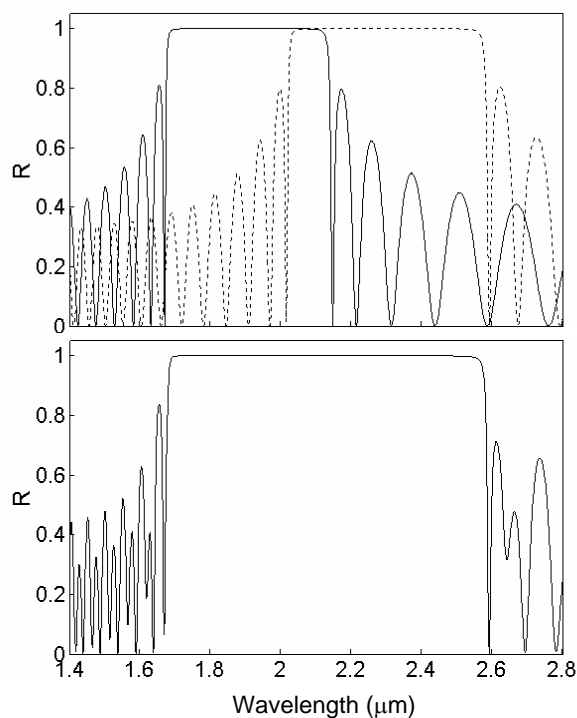


Fig. 3.13. Reflectivity spectrum of a) two DBR with $n_H=2.3$, $n_L=1.6$ and $N=20$. One of them is formed by layers with optical thickness $\lambda/4=1.88 \mu\text{m}/4$, and the other is formed by layers with optical thickness $\lambda/4=2.27 \mu\text{m}/4$. b) DBR with 40 periods and $n_H=2.3$, $n_L=1.6$ consisting of the two DBRs stacked together.

Fig. 3.13a shows the reflectivity spectrum, for normal incidence, of two DBR with the same refractive indices and the same number of periods. On the contrary, the thicknesses of the layers are different for each DBR, and therefore their bandgaps are centered at different wavelengths. We can observe that the bandgaps intersect. Fig. 3.913b shows the reflectivity spectrum of a multilayer formed by the two DBR stacked together. We can see that its bandgap is the union of the bandgaps of the DBRs presented in Fig. 3.913a .

Although, in this example, the filters have the same refractive indices and different thicknesses, it could be possible to use different refractive indices and/or thicknesses. One of the aims of the stack of filters is the widening of the DBR bandgap but it could be also used for obtaining a DBR with high reflectivity at separated wavelength ranges. In this case, the stacked filters should have bandgaps situated at the desired wavelength ranges.

3.3.2. Microcavities

It is possible to fabricate a particular class of interferometers, named microcavities or Fabry-Pérot filters, by using two parallel reflectors separated by a spacer layer. Usually the reflectors used are $\lambda/4$ DBR. The reflectivity spectrum of microcavities consists of a wide high-reflectivity bandgap with a narrow pass-band in its center. The wavelength at which this pass-band (also called transmission peak) is situated, its width and its reflectivity level depend on different parameters.

3.3.2.1. Performance of the developed programs for the simulation of microcavities

Microcavities are multilayer structures widely studied for many different applications. We use here a porous silicon microcavity reported in [78] to evaluate the performance of the simulation programs. The microcavity consists of two $\lambda/4$ -DBR with 4 periods where $n_H=2.24$ and $n_L=1.27$. The optical thickness of the layers are $\lambda/4= n_H d_H=n_L d_L$ with $\lambda =600$ nm. The spacer layer

thickness is $\lambda/2$ and its refractive index is $n_s=1.27$. Fig. 3.14 shows the simulated reflectivity spectrum of this multilayer where we can observe that it completely agrees with the reflectivity spectrum reported in [78].

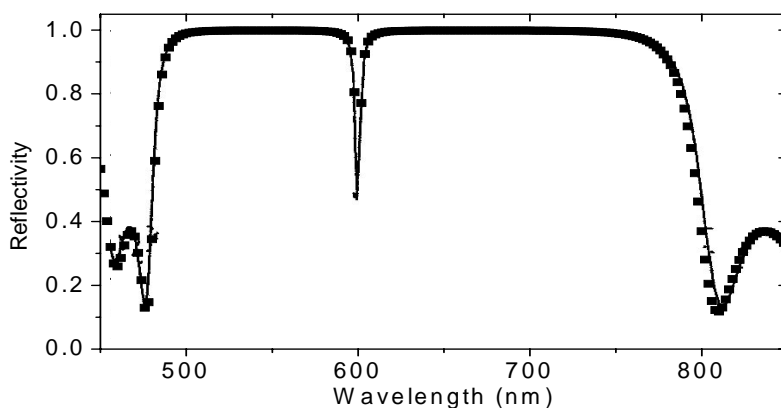


Fig. 3.14. Reflectivity spectrum simulated with our program (symbols) and simulated reflectivity spectrum of the same microcavity structure reported in [78].

3.3.2.2. Study of the microcavity parameters

The influence of the different parameters of microcavities on the reflectivity spectrum has been also studied.

a) Thickness of the spacer layer (h_s)

Whereas the optical thickness of the DBRs are usually $\lambda/4$, the optical thickness of the spacer layer can be either λ or $\lambda/2$. In both cases, the transmission peak is centered at wavelength λ . The reflectivity spectra of microcavities with a λ or a $\lambda/2$ spacer layer are compared in Fig. 3.15. This figure shows the reflectivity spectra for normal incidence of microcavities consisting of two parallel DBR with 6 periods and optical thickness $\lambda/4$, where $\lambda=1.55 \mu\text{m}$. In Fig. 3.15a, the optical thickness of the spacer is λ , whereas in

Fig. 3.15b this thickness is $\lambda/2$. Both spectra are very similar. The transmission peak is centered at $1.55 \mu\text{m}$ in both cases and the reflectivity for both is almost zero at this wavelength. However, the bandgap of the microcavity with the $\lambda/2$ spacer is slightly wider than the one with thickness λ and the side-lobes closer to the bandgap show a lower reflectivity.

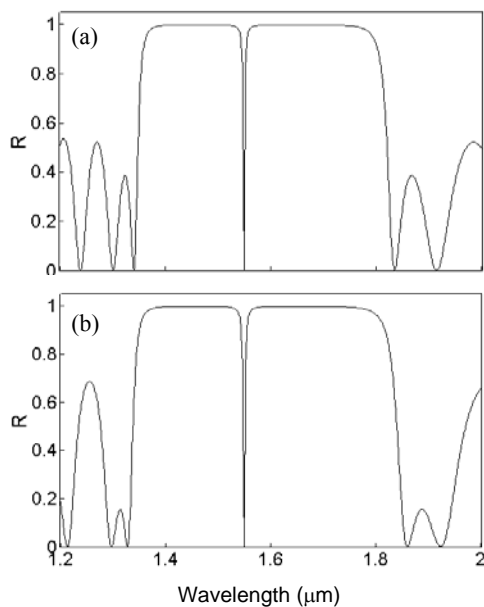


Fig. 3.15. Reflectivity spectrum of a microcavity consisting of two DBR with optical thickness $\lambda/4$ and a spacer layer of thickness a) λ , b) $\lambda/2$.

b) Refractive index of the spacer layer

The refractive index of the spacer layer can be one of the indices used in the DBRs (n_H, n_L) of the microcavity or a different value. The influence of this value on the reflectivity spectrum of the microcavity has been studied for all the possible cases: for a refractive index lower than n_L , equal to n_L , between n_L and n_H , and equal to n_H . The results can be observed in Fig. 3.16. The four plots belong to porous silicon microcavities for $1.55 \mu\text{m}$ applications. The $\lambda/4$ -DBRs

that form them have $n_L=1.6$, $n_H=2.3$ and $N=6$. The spacer thickness is $\lambda/2$ and its index n_s is 1.4 ($n_s < n_L$), 1.6 ($n_s = n_L$), 1.8 ($n_L < n_s < n_H$), and 2.3 ($n_s = n_H$). The transmission peak is positioned for all of them at $1.55 \mu\text{m}$ and its reflectivity is almost zero for all, therefore we can deduce that the refractive index of the spacer does not noticeable affect the bandgap or the transmission peak. The difference between these spectra is observed at the side-lobes.

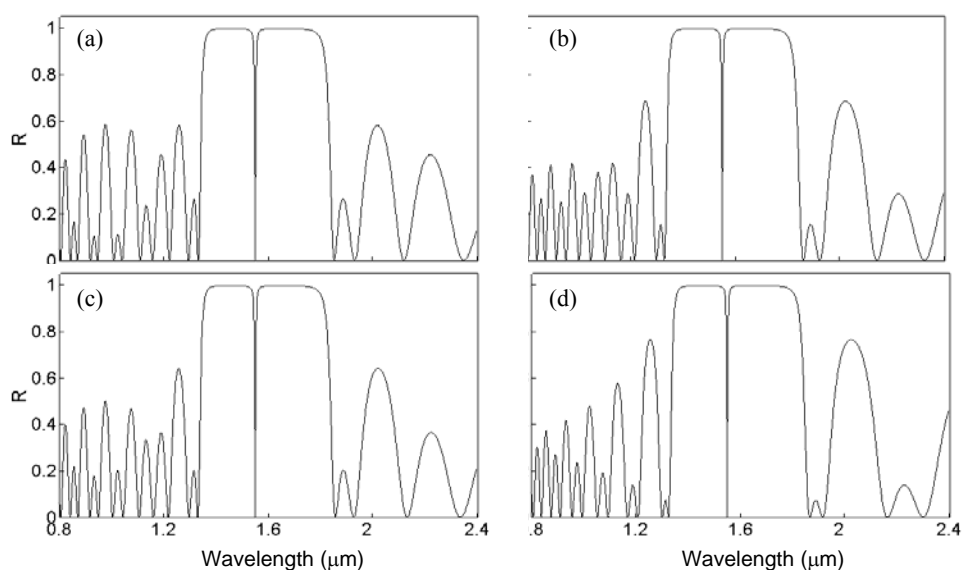


Fig. 3.16. Reflectivity spectrum of a microcavity consisting of two DBR with $n_L=1.6$ and $n_H=2.3$. The thickness of the spacer layer is $\lambda/2$ and its refractive index is a) 1.4, b) 1.8, c) 1.6 d) 2.3.

c) Number of periods of the DBR

The width of the transmission peak depends on the number of periods N of the DBRs of the microcavity. When N increases, the transmission peak becomes narrower, the reflectivity of the bandgap increases and its edges are sharper. These effects can be observed in Fig. 3.17.

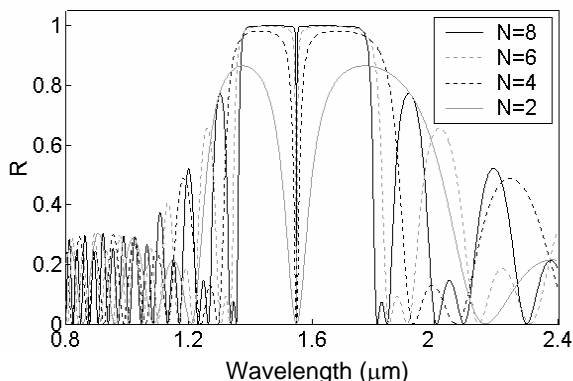


Fig. 3.17. Reflectivity spectrum of a porous silicon microcavity for 1.55 μm applications where the DBRs that form it have a different number of periods.

3.4. Summary and conclusions

We have demonstrated that the transfer matrix method is a very useful and simple mathematical method for the simulation of multilayers. Very user-friendly programs based on this method have been developed and all their variable parameters have been explained. They calculate the reflectivity, transmission and absorption spectra; and the photonic band diagrams of multilayers. The parameters that can be adjusted by the used are the refractive index and thickness of the layers, the number of periods, the incidence angle and the wavelength range. Besides, one of the programs can be used for the study of different periodic multilayers stacked together.

Although the simulations realized during this work have been focused on porous silicon layers, any other material could be simulated because the user can select the refractive indices. These refractive indices can be either constant (real or complex) or variable with wavelength, in which case different materials can be selected (Ag, Al, Au, Cu, MgF_2 , Ni, Si_3N_4 , and SiO_2). The number of selectable materials will be increased in a near future.

To evaluate the performance of the developed programs we have simulated different Distributed Bragg Reflectors (DBR) and microcavities. The

simulated spectra agree with the ones reported in the literature, which indicates the suitability of the developed programs. With the study of DBRs, we have observed that porous silicon is a suitable material for the fabrication of filters with a wide bandgap centered at $\lambda=1.55 \mu\text{m}$. This bandgap can be wider with the fabrication of porous silicon stacked filters. The introduction of defect layers in the DBR has led to the study of microcavities and the understanding of the effect of these layers on the reflectivity spectrum of the multilayer structure.